CO2 thermal infrared signature following a sprite event in the mesosphere

Frédéric Romand, Anne Vialatte, Laurence Croizé, Sébastien Payan, M. Barthelemy

Journal of Geophysical Research: Space Physics

RESEARCH ARTICLE
10.1029/2018JA025894

Key Points:
- Sprite thermal infrared signature could reach up to 10^{-7} W/sr/cm^2/cm^{-1} for an observer located in the stratosphere
- The maximum signal is in the long-wavelength infrared, around 1,000 cm^{-1}
- This signature should be detectable from stratospheric balloons

Correspondence to:
F. Romand,
frederic.romand@protonmail.com

Citation:
Romand, F., Vialatte, A., Croizé, L., Payan, S., & Barthélémy, M. (2018). CO_2 thermal infrared signature following a sprite event in the mesosphere. *Journal of Geophysical Research: Space Physics*, *123*, 8039–8050. https://doi.org/10.1029/2018JA025894

Received 13 JUL 2018
Accepted 12 SEP 2018
Accepted article online 15 SEP 2018
Published online 28 SEP 2018

CO_2 Thermal Infrared Signature Following a Sprite Event in the Mesosphere

Frédéric Romand[1,2], Anne Vialatte[2], Laurence Croizé[1], Sébastien Payan[2], and Mathieu Barthélémy[3]

[1]ONERA-DOTA-MPSO, Palaiseau, France, [2]LATMOS, Paris, France, [3]IPAG, UMR 5274, UFR Phitem, Université Grenoble Alpes/CNRS-INSU, Grenoble, France

Abstract Sprites are a potential thermal infrared radiation source in the stratosphere and mesosphere through molecular vibrational excitation. We developed a plasma-chemical model to compute the vibrational kinetics induced by a sprite streamer in the 40- to 70-km altitude range until several tens of seconds after the visible flash is over. Then, we computed the consecutive time-dependent thermal infrared spectra that could be observed from the stratosphere (from a balloon platform), high troposphere (from an aircraft), and low troposphere (aircraft or altitude observatory) using a nonlocal thermodynamic equilibrium radiative transfer model. Our simulations predict a strong production of CO_2 in the (001) vibrational level which lasts at least 40 s before falling to background concentrations. This leads to enhanced emissions in the long-wavelength infrared, around 1,000 cm^{-1}, and midwavelength infrared, around 2,300 cm^{-1}. The maximum sprite infrared signatures (sprite spectra minus background spectra) reach several 10^{-7} W/sr/cm^2/cm^{-1} after propagation through the mesosphere and stratosphere, to an observer located at 20–40 km of altitude. This maximum signal is about 1 order of magnitude lower if propagated until the troposphere. From the two spectral bands, the 1,000-cm^{-1} one could be detected more easily than the 2,300-cm^{-1} one, which is more affected by atmospheric absorption (CO_2 self-trapping at all altitudes and H_2O mostly in the troposphere). With a sufficiently sensitive instrumentation, mounted in an open stratospheric balloon platform for example, the 1,000-cm^{-1} band could be detected from 20–40 km of altitude.

1. Introduction

Transient luminous events (TLEs) are electrical and optical phenomena that occur above thunderstorms from 15 to 110 km (Pasko et al., 2012). Their occurrence is related to the electrical activity underlying thunderstorms in the troposphere and lower stratosphere (Wilson, 1924). Sprites are the most documented type of TLEs; they develop mainly downward from the base of the ionosphere (Pasko, 2010), cover altitudes from 40 to 90 km, and have a typical vertical extension of 40 km for a 5- to 30-km width (Sentman et al., 1995). Sprites were first recorded by accident in 1989 (Franz et al., 1990); since then, their visible, ultraviolet, and near-infrared (NIR) emissions have been observed and studied. Above 80 km, the reddish optical emissions of the diffuse region were related to the first positive band of N_2 (1P(N_2)): N_2 ($B^3\Pi_g$) → N_2 ($A^3\Sigma_u^+$) (Hampton et al., 1996; Mende et al., 1995). Below 75 km, the streamer region is characterized by tendrils and blueish emissions (Pasko et al., 2002; Pasko & Stenbaek-Nielsen, 2002). These ones were identified coming from the second positive band of N_2: N_2 ($C^3\Pi_u$) → N_2 ($B^3\Pi_g$), and first negative band of N_2^+: $N_2^+(B^2\Sigma_u^+)$ → $N_2^+(X^2\Sigma_g^+)$ (Armstrong et al., 1998; Morrill et al., 1998). Some Meinel emissions ($N_2^+(A^2\Pi_u)$ → $N_2^+(X^2\Sigma_g^+)$) were found to be detectable at low altitudes (Bucsela et al., 2003). Siefring et al. (2010) identified OH airglow and 1PN_2 transitions in NIR spectra (888 and 1,050 nm) from images acquired during the Energetics of upper atmospheric eXcitation by Lightning airborne campaign. Sprites spectra have been calculated in the NIR and near ultraviolet for different observation configurations: altitude observatory (3.25 km), airplanes (14 km), balloons (35 km), and space (for a nadir line of sight [LOS]) by Gordillo-Vázquez et al. (2012). Particularly pronounced sprite signatures were found in the NIR region at 1,046 and 1,231 nm (1PN_2 transitions).

Different authors have highlighted the potential thermal infrared (TIR) emissions of sprites. Milikh et al. (1998) evaluated the 4.26-μm band emissions. Their model considered the generation of molecular nitrogen vibrational levels followed by the transfer to CO_2(001) and the subsequent IR photons emissions. Their propagation through the atmosphere, optically thick, has shown that the IR detection should be realized from space. Later on, Gordillo-Vázquez (2008) proposed a plasma kinetic model of about 500 reactions. Considering the vibrational kinetics of N_2 and CO_2 following the passage of a sprite streamer at a given

altitude (pulse phase), he explicitly evaluated the radiative emissions of CO_2 in the IR between 63 and 78 km of altitude. Right at the end of the pulse, at 63 and 68 km, the 4.23-μm emissions exhibited an abrupt increase that was much smoother at 78 km. The enhancement ranged from 3 orders of magnitude (78 km) to more than 6 orders of magnitude (63 km). The maximum emissions were reached well after the pulse is over (1 ms at 63 km, 10 ms at 68 and 78 km) and persisted for several seconds. Then, Parra-Rojas et al. (2015), used a one-dimensional self-consistent model to study the chemical and thermal effects of a single sprite streamer in the mesosphere. The 4.26-μm IR emissions of CO_2 were found to reach 10 GR at low altitudes ($<$ 65 km). These results suggested the possibility of detecting sprite IR emissions from space or aircrafts with the appropriate instrumentation.

The Atmospheric Space Interaction Monitor is a climate observatory for the International Space Station (ISS). It was launched on 2 April 2018. Its payload is composed of an X and gamma ray detector and an optical instrument consisting of two cameras and four photometers pointing to the nadir (asim.dk). After 2 months of commissioning, it is now in operation. It is used to study TLEs and terrestrial gamma ray flashes. The Tool for the Analysis of Radiations from lightNings and Sprites is a Centre National d'Etudes Spatiales, French space agency microsatellite (Lefeuvre et al., 2008). It is scheduled to be launched in late 2019 (Taranis.cnes.fr). Its main objective is to study impulsive transfers of energy between the Earth atmosphere and the space environment. It is equipped with an optical instrument composed of two cameras and four photometers (Farges et al., 2017). None of these missions will record spectrally resolved radiances and any IR signatures of sprites.

The High Altitude Luminous Events Studied by spectro-Imagery (HALESIS) project, presented in Croize et al. (2015), aims to load a spectroimager on board a stratospheric balloon in order to obtain hyperspectral IR images of the atmosphere locally disturbed by a TLE in the seconds following the visible flash. In order to evaluate the requirements of the instrument to be used and the optimized geometry of observation, it is necessary to characterize the potential IR sources in TLEs and to propagate it through the atmosphere to an observer with an oblique LOS.

This paper provides a contribution to the understanding of the vibrational kinetics caused by a sprite streamer and the subsequent emissions in the TIR propagated through the middle atmosphere toward an observer located in the stratosphere. In section 2, the plasma-chemical model developed is presented. It computes the enhancement of electron concentrations and the following vibrational kinetics consecutive to the pulse generated by a sprite streamer at a given altitude in the mesosphere. The duration of the pulse phase is evaluated with respect to the similarity law which connects the concentration of electrons inside the streamer head at a given altitude to that of laboratory streamers at ground pressure (Qin & Pasko, 2015). In section 3.1, the time evolution concentrations of electrons, first eight vibrational levels of N_2, and first level of each vibrational mode of CO_2 are presented until its fall to background concentrations. Then, for the first time, the CO_2 vibrational populations are used to compute the sprite-disturbed atmospheric emissions at around 1,000 and 2,300 cm^{-1} propagated through the atmosphere to an observer located in the stratosphere (HALESIS-type setup). This is presented in section 3.2. The signatures are computed for an observer located at typical altitudes of open stratospheric balloons (OSB, 40 km), a widely used platform in atmospheric studies (Camy-Peyret et al., 1995; Friedl-Vallon et al., 1993) and the principal flight solution considered for the HALESIS project. If using an OSB platform, the balloon should be launched specifically when a thunderstorm happens (or for a high forecast). The instrument should be as close as possible from a potential sprite event but not too close to avoid a flight above the thunderstorm, where strong convection and electrical activity could damage the balloon and payload during the ascension phase. An alternative study is done from the altitude of high-altitude platform system (HAPS; d'Oliveira et al., 2016). Let us cite, for example, Stratobus, a project of HAPS developed by Thales Alenia Space. When operational, it will go on stationary flights at 20 km of altitude, in tropical regions. It will achieve civilian and military missions in the field of observation and communication (Baurreau et al., 2015). In the case of the HAPS platform, the balloon remains in flight for months and constantly stays above the same point on the ground. The aircraft will not necessarily be at a suitable distance from the thunderstorm. As a comparison, the signatures are also computed for altitude observatories (3,000 and 5,000 m) and plane altitude (10,000 m). These computations are done using a nonlocal thermodynamic equilibrium radiative transfer model and will contribute to the definition of mission specifications in the framework of the HALESIS project. Finally, the main contributions presented in this work are summarized in the last section together with the main perspectives.

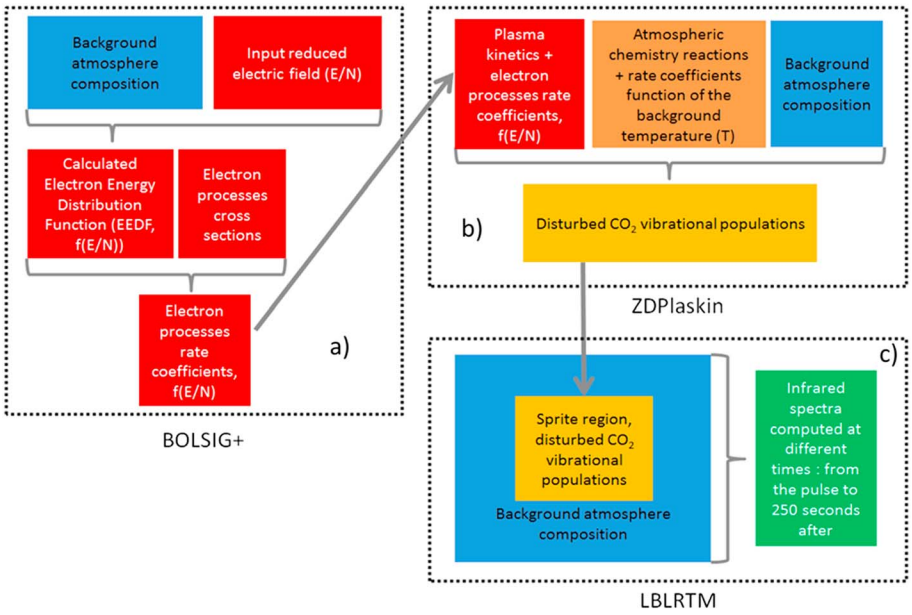

Figure 1. Computation pipeline for the simulation of the plasma kinetics of a sprite streamer and subsequent time-dependent thermal infrared radiative emissions. (a) Stands for the plasma parameters computation, (b) for the solving of the kinetic scheme, and (c) for the radiative transfer computations.

2. Materials and Methods

To compute the sprite IR signature, the coupling of a plasma-chemical model and a radiative transfer model is required. The overall computation pipeline consists of three steps: the computation of the plasma parameters, the solving of the plasma/chemical kinetics, and the spectra computations (Figure 1).

The input atmospheric composition values comes from the Whole Atmosphere Community Climate Model (Marsh et al., 2013). It contains vertical temperature and concentration profiles of the following species: CO, CO_2, H, H_2, H_2O, H_2O_2, HNO_3, HO_2, N, N_2O, NO, NO_2, NO_3, O, O_2, O_3, and OH. Standard midlatitude (45° of latitude, 0° of longitude) nighttime (midnight local time) mean summer conditions are used in our study. Initial electron (Hu et al., 2007) and O_2^+ vertical concentration profiles are also included in our model and are identical to respect global neutrality:

$$\sum_j n_j^+ = n_{e^-} + \sum_k n_k^-, \tag{1}$$

with n_j^+, n_{e^-}, and n_k^- being the total number of positive ions, electrons, and negative ions, respectively. The initial populations of excited levels of molecules are supposed to be at local thermodynamic equilibrium (LTE). Thus, the initial concentrations of excited species included in the kinetic model are defined following a Maxwell-Boltzmann distribution:

$$n_{\mathrm{exc}} = n_0 \frac{g_{\mathrm{exc}}}{g_0} e^{(-h\nu/kT)}, \tag{2}$$

with n_{exc} being the concentration of an excited species, n_0 the concentration of the ground state, g_{exc} and g_0 the degeneracies of excited and ground species, respectively, h Planck's constant, ν the frequency of the excited level, k the Boltzmann constant, and T the temperature.

The modeling of the plasma-chemical kinetics is based on the sprite streamer model of Gordillo-Vázquez (2008). This model considers 77 species and almost 500 reactions.

This scheme contains Electron Energy Distribution Function (EEDF) and electron temperature (T_e) dependent processes, both directly related to the applied reduced electric field (E/N), heavy particle chemistry, vibrationally and electronically excited species chemistry, ionic chemistry, and radiative processes. The rate

coefficients of all these processes are provided by Gordillo-Vázquez (2008), except for the plasma-chemistry EEDF-dependent set. These latter have to be computed since they depend on the applied *E*/*N*. This is done using BOLSIG+ 03/2016 version (Hagelaar & Pitchford, 2005), a Boltzmann equation solver, as summarized in Figure 1a. The whole computation procedure of the plasma parameters is detailed in the user's manual of the code (https://www.bolsig.laplace.univ-tlse.fr/manual).

To simplify the model and to gain on numerical stability, the humid air chemistry of Gordillo-Vázquez (2008) is not included (the author investigated the effects of air humidity, which is out of the scope of the present paper). The model considers the first level of each vibrational mode of CO_2: 010, 100, and 001 since they are involved in the main TIR emission processes. The populations of these levels are governed by interactions involving electrons, vibrational N_2, main background molecules, and radiation. Direct impacts with electrons and spontaneous emission are already included, likewise vibration-vibration (V-V) exchanges between N_2(v1) and CO_2(001) and vibration-translation (V-T) exchanges between N_2 (v = 1, …,8) and fundamental N_2. In order to complete the vibrational kinetics and to describe the quenching of vibrational levels, we updated the kinetic scheme with V-V transfers between N_2(v = 2, …, 8) and CO_2(v) and V-T transfers between vibrational (N_2, CO_2) and background atmosphere (O, O_2, CO, CO_2, N, and N_2). These processes and related rate coefficients are from Parra-Rojas et al. (2015).

Before starting a sprite simulation, the model runs several minutes without any electric field (*E*/*N* = 0) to ensure the concentrations are steady in the absence of a sprite. This stage corresponds to Figure 1b, disabling the plasma kinetics set of reactions. The kinetics triggered by a sprite streamer is described by Sentman et al. (2008) as follows. A descending streamer head impulsively ionizes the atmosphere, leaving in its path a large amount of electrons, ions, and excited molecular or atomic states. Inside the tail following the passage of the head, the trailing column, electrons can persist for about 1 s at 70 km.

Our sprite streamer kinetics simulation consists of two stages. The first one is called the pulse. An electric field of 400 Townsends (corresponding to a mean electron temperature of 6.29 eV) is applied for a duration varying with the altitude. This corresponds to the passage of a streamer head. According to Qin and Pasko (2015), the concentration of electrons reached in a sprite streamer head follows the similarity law:

$$e_h \propto \left(\frac{N_h}{N_0}\right)^2 \tag{3}$$

with e_h being the concentration at a given altitude h, N_h the concentration of neutral species at the altitude h, and N_0 the concentration of neutral species at altitude 0. The concentration of electrons reached at ground pressure (e_0) is 10^{14} cm^{-3} so that

$$e_h = e_0 . \left(\frac{N_h}{N_0}\right)^2 . \tag{4}$$

Knowing the total ionization and attachment rates for a reduced electric field of 400 Td (based on plasma parameters computation), we estimated the duration of the pulse needed to obtain the concentration of electrons given by equation (4) and found 3.9×10^{-7}, 1.2×10^{-6}, 3.5×10^{-6}, and 9.6×10^{-6} s, respectively, at 40, 50, 60, and 70 km of altitude.

The second stage, called the relaxation, lasts 250 s during which an *E*/*N* of 30 Td is still applied. This value corresponds to the quasi-electrostatic field maintained above thunderstorms (Picard et al., 1997).

The kinetics is solved with an altitude step of 1 km through the relation

$$\frac{\partial n_s}{\partial t} = G_s - L_s, \tag{5}$$

where n_s is the concentration of each species, and G_s the gain processes and L_s the loss processes using ZDPlaskin code (Pancheshnyi et al., 2008).

Since BOLSIG+ is also included in ZDPlaskin as a module, it would have been possible to compute the EEDF, T_e, and the plasma rate coefficients at each time step of the kinetics resolution. However, the plasma parameters are computed preliminary and used as tabulated inputs. In this way, the computation is simplified and faster.

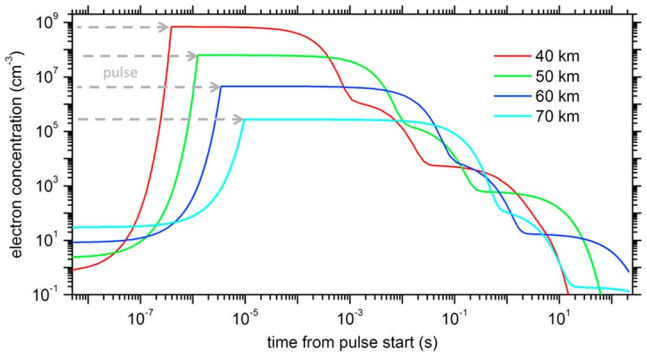

Figure 2. Time evolution of the electron concentrations from 40 to 70 km of altitude. The durations of the pulse phases are represented by gray dashed arrows.

At the end of the plasma and kinetics computations, we obtain the time evolution of the concentrations of vibrational CO_2, which can be converted in vibrational temperatures (T_{vib}). The objective is to use these sprite-disturbed T_{vib} to evaluate the associated radiative disturbances, in the 800- to 2,500-cm^{-1} spectral range, at different times after the pulse is over until return to background kinetic temperature.

To do so, the outputs of the model are coupled with the Line By Line Radiative Transfer Model (Clough et al., 2005; Figure 1c). Line By Line Radiative Transfer Model is capable of nonlocal thermodynamic equilibrium computations so that the vibrational temperatures of each level of different species (H_2O, O_3, CO, NO, and CO_2) can be individually considered (assuming a rotational LTE).

To simulate the presence of a sprite, we determine what volume of atmosphere is distured by streamers during an event. The total number of streamers composing a sprite is about several thousands, and their dimension ranges from tens to hundreds of meters of diameter (Arnone et al., 2014; Pasko et al., 2012). Thus, we assume that the total volume disturbed by the kinetics of sprite streamers, in the streamer region (Pasko & Stenbaek-Nielsen, 2002), can be represented by a single equivalent cylinder of 5 to 20 km of diameter and 30 km high, covering the altitudes between 40 and 70 km.

At each time t_x at which we want to obtain the radiative signature, we apply the streamer-disturbed T_{vib} of vibrational CO_2 of the corresponding time to the equivalent sprite volume. On the vertical dimension, the altitude-dependent CO_2 T_{vib} are applied. On the horizontal dimension, this disturbance is assumed to be uniform.

Four values will be used to define the geometrical setup of the radiance computations. Three values define the LOS: h_o, the altitude of the observer, d, the horizontal distance between the observer and the edge of the sprite region, h_s, the altitude at which the LOS crosses the sprite. The last one corresponds to the width of the sprite, l.

3. Results

This section is dedicated to the presentation and the discussion on the results of the two main aspects of this work: the vibrational kinetics of CO_2 following the disturbance induced by a sprite streamer and the related TIR emissions until its fall back to background values.

3.1. Vibrational Kinetics

The population of CO_2 vibrational levels comes from two kinds of processes: direct impacts with electrons and vibration-vibration exchanges with vibrational levels of N_2. As a validation purpose, we first performed our calculations for the same initial conditions and parameters as those used by Gordillo-Vázquez (2008) and found similar results. The model used in the present work stands out from that of Gordillo-Vázquez (2008) in terms of the initial atmospheric composition, initialization of excited species concentrations, vibrational kinetics set of reactions, cross sections used to compute the plasma-kinetics EEDF-dependent rate coefficients, duration of the pulse phase, and electric field value during the relaxation phase (see section 2). Thus, we will describe the production of electrons, vibrational N_2, and, finally, vibrational CO_2 obtained with the conditions and parameters described in section 2.

The gain and loss processes of electrons are discussed in detail in Gordillo-Vázquez (2008). Our electron kinetics being the same, we do not discuss it further. The resulting electron time evolutions, which differs from Gordillo-Vázquez (2008) because of our use of an altitude dependent pulse duration, are presented in Figure 2.

The rapid enhancement of the electron concentration corresponds to the passage of the streamer head. The maximum value is imposed by the duration of the pulse, which is an input parameter. The following plateau corresponds to the trailing column phase, as described in Sentman et al. (2008). The duration of the plateau at 70 km is similar to that of Sentman et al. (2008), who computed the effects of a streamer at this same altitude.

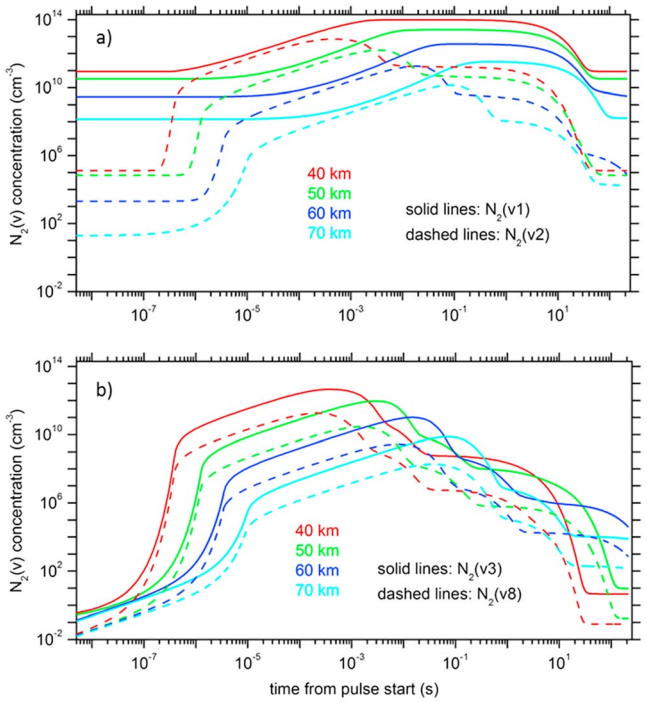

Figure 3. Time evolutions of the concentrations of N_2 vibrational levels from 40 to 70 km of altitude. Panel (a) shows the concentrations of the first and second N_2 vibrational levels. Panel (b) shows the concentrations of the third and eighth N_2 vibrational levels.

At lower altitudes, this phase is shorter since loss processes (attachment and recombination) rates are increased by pressure: it varies from 10^{-4} to 0.1 s from 40 to 70 km.

These electron time evolutions affect CO_2 vibrational levels through P1 to P3 direct impact processes:

$$CO_2(000) + e \leftrightarrow CO_2(010) + e, \quad \text{(P1)}$$

$$CO_2(000) + e \leftrightarrow CO_2(100) + e, \quad \text{(P2)}$$

$$CO_2(000) + e \leftrightarrow CO_2(001) + e, \quad \text{(P3)}$$

and the populations of $N_2(v)$ through P4 and P5 direct impact processes:

$$N_2(v_0) + e \leftrightarrow N_2(v_i) + e, \text{with } i = 1, \ldots, 8 \quad \text{(P4)}$$

and

$$N_2(v_j) + e \leftrightarrow N_2(v_{j+1}) + e \text{ with } j = 1, \ldots, 7. \quad \text{(P5)}$$

$N_2(v)$ populations are also influenced by a set of V-T and V-V processes:

$$N_2(v_1) + N_2(v_i) \leftrightarrow N_2(v_0) + N_2(v_{i+1}), \text{with } i = 1, \ldots, 7, \quad \text{(P6)}$$

$$N_2(v_j) + M \leftrightarrow N_2(v_{j-1}) + M, \text{with } M = (N_2(v_0), O, N) \text{ and } j = 1, \ldots, 8, \quad \text{(P7)}$$

$$N_2(v_1) + CO_2(000) \leftrightarrow N_2(v_0) + CO_2(000), \quad \text{(P8)}$$

and

$$N_2(v_i) + CO_2(000) \leftrightarrow N_2\ (v_{i-1}) + CO_2(001), \text{with } i = 1, \ldots, 8. \quad \text{(P9)}$$

These processes lead to the time evolutions presented in Figure 3. The $N_2(v_1)$ level shows an increase of up to 4 orders of magnitude from 40 to 70 km and falls to background values after 35 to 100 s, respectively. The $N_2(v_2)$ level rapidly increases 5 orders of magnitude within 5×10^{-7} to 10^{-5} s from 40 to 70 km of altitude. A second phase of increase follows so that the concentrations reach 3 to 4 orders of magnitude more. $N_2(v_3)$ to $N_2(v_4)$ levels shows similar trends with a stronger first phase of increase which is about 7 to 10 orders of magnitude from 70 to 40 km of altitude. Moreover, this increase lasts 5×10^{-7} to 10^{-5} s from 40 to 70 km of altitude.

The gap of energy between two N_2 vibrational levels is of 0.29 eV. Thus, the CO_2(001) level, which energy is 0.29 eV too, is efficiently populated by vibration-vibration exchanges with $N_2(v)$ (P9 process). The CO_2 (001) enhancement is represented in Figure 4.

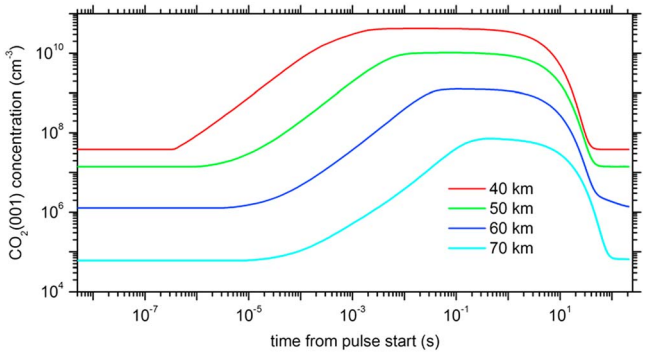

Figure 4. Time evolution of the concentration of CO_2(001) level from 40 to 70 km of altitude.

CO_2 (001) concentration gains 3 orders of magnitude before falling to background concentrations within 35 s at 40 km and about 100 s at 70 km due to collisional quenching (P10):

$$CO_2(v_{high}) + M \leftrightarrow CO_2(v_{low}) + M, \quad \text{(P10)}$$

with v_{high} an upper vibrational level (001, 100 or 010), v_{low} a lower vibrational level (100 or 010) or the fundamental CO_2, and M = (CO_2, N_2, O, CO, O_2), and radiative deexcitation (R1 and R2):

$$CO_2(001) \rightarrow CO_2(100) + h\nu_1, 1063\ cm^{-1} \quad \text{(R1)}$$

$$CO_2(001) \rightarrow CO_2(000) + h\nu_2, 2347\ cm^{-1} \quad \text{(R2)}$$

$$CO_2(100) \rightarrow CO_2(010) + h\nu_3, 719\ cm^{-1} \quad \text{(R3)}$$

$$CO_2(010) \rightarrow CO_2(000) + h\nu_4, 671\ cm^{-1} \quad (R4)$$

the second column being the emitted photon wavenumber. The consecutive populations of CO_2(010) and CO_2(100) comes from the cascading transfer of vibration from a highly excited level, to a lower level (P11, P12):

$$CO_2(001) + CO_2 \leftrightarrow CO_2(100) + CO_2(010), \quad (P11)$$

$$CO_2(100) + CO_2 \leftrightarrow CO_2(010) + CO_2(010), \quad (P12)$$

and radiative deexcitation (processes R1, R3, and R4). The rate coefficients of these two last processes (P11, P12) being about the order of 10^{-11} cm^3/s, there is no significant production of (010) and (100) levels. The enhancement of their concentration is less than a factor 1.5 at all altitudes.

The concentrations can be expressed as vibrational temperatures, which will be used to characterize the chemical disturbance in the computations of sprite spectra:

$$\Delta T_{vib} = T_{vib}^{max} - T_{kin} \quad (6)$$

with ΔT_{vib} the disturbance in kelvin, T_{vib}^{max} the maximum vibrational temperature reached after the pulse (typically after 1 s), and T_{kin} the background kinetic temperature. For (001) level, ΔT_{vib} is equal to 255, 246, 215, and 168 K, respectively, for 40, 50, 60, and 70 km (corresponding to an enhancement of about 3 orders of magnitude in concentration). For (010) and (100) levels, the disturbance is never greater than several kelvins.

As a conclusion, this kinetic model of sprite streamer, adapted from that of Gordillo-Vázquez (2008), completed with vibrational processes from Parra-Rojas et al. (2015), and applied with an altitude-dependent pulse duration, leads to no significant disturbance of (010) and (100) levels and 168 to 255 K of ΔT_{vib} for (001) from 70 to 40 km. The disturbance obtained for CO_2(001) is of the same order of magnitude than that of Parra-Rojas et al. (2015) at comparable altitudes (50–70 km; the authors did the computations between 50 and 80 km). Considering the processes of deexcitation of this level, R1 and R2, the significant radiative perturbation will be localized near 1,063 and 2,347 cm^{-1} (9.4 and 4.6 μm) in the simulated spectra. The next section will provide the intensity of different cases of sprites TIR signatures, and different geometries of observation will be simulated.

3.2. Radiative Transfer

We will first present the radiance computations in the framework of the HALESIS experiment for two kinds of platforms: OSB (30–45 km of flight altitude) and HAPS (20 km of flight altitude). We will also present the signatures for observers located at altitude observatories levels, 3,000 and 5,000 m, and from a typical aircraft level (10 km).

The geometrical parameters of the future HALESIS balloon experiment case are as follows: the observer is located at 40/20 km of altitude (OSB and HAPS cases, respectively), 50 km of horizontal distance from a sprite of 10 km width, and the altitude at which the LOS crosses the sprite is 50 km (h_o = 40/20 km, d = 50 km, l = 10 km, h_s = 50 km, Figure 5). A spectral resolution of 1 cm^{-1} is used in the following plots.

For the OSB observer case (Figures 5a and 5b), two distinct sets of P and R branches grow from the R1 process in the long-wavelength infrared (LWIR), between 900 and 1,100 cm^{-1}. In the midwavelength infrared (MWIR) region, between 2,200 and 2,400 cm^{-1}, the signature (subtraction of the background spectrum to the sprite spectrum) comes from the R2 process. The shape of the branches is not defined as well since it corresponds to a strong atmospheric absorption band. Thereafter, we call the LWIR and MWIR bands R1 and R2 spectral bands, respectively.

Time evolutions of the signatures show the amplitude decay of the signal until 40 s. At 50 s, there is no more contribution of the sprite to the spectrum. The maximum signatures, at 1 s, are about 2×10^{-7} and 2.4×10^{-8} $W/cm^2/sr/cm^{-1}$ in R1 and R2 bands, respectively. At 40 s, the signatures are about 3×10^{-10} and 5×10^{-11} $W/cm^2/sr/cm^{-1}$ in R1 and R2 bands, respectively. Thus, the signal decrease is of almost 3 orders of magnitude in 40 s (Figure 5b). This is predicted by the kinetics of CO_2 (001) levels at 50 km (altitude at which the LOS crosses the sprite), as presented in Figure 4. It shows the fall of this level to background concentrations between 40 and 50 s.

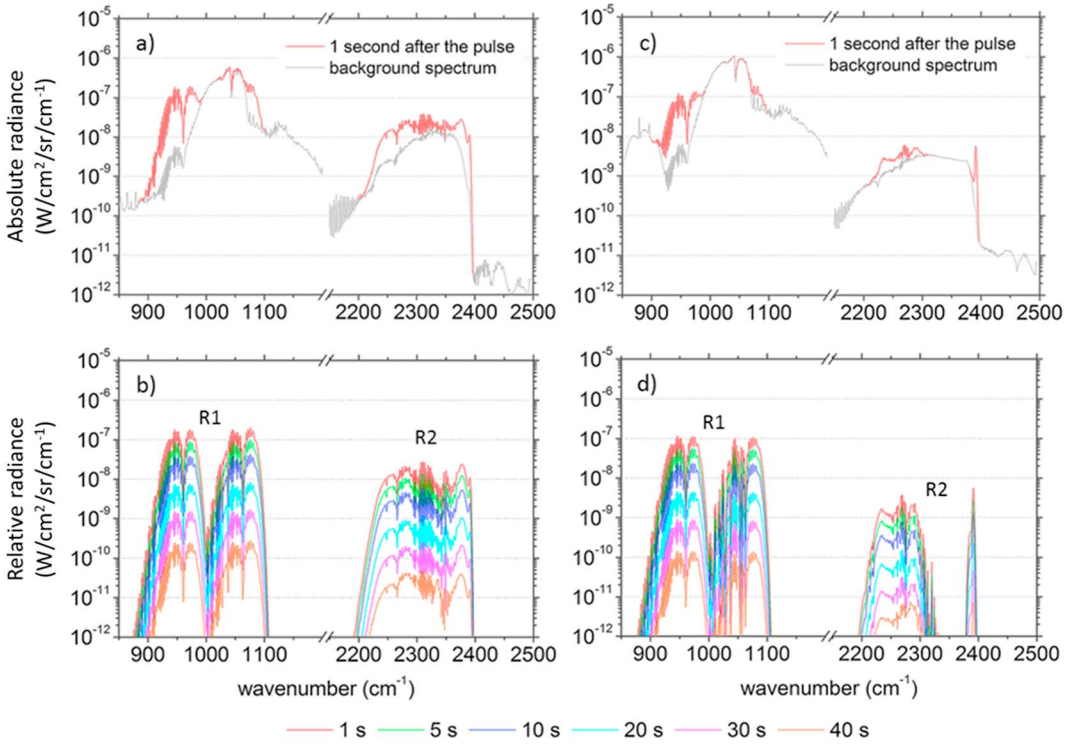

Figure 5. Absolute spectra of background atmosphere, in gray, and sprite, in red, for an observer located at 40 and 20 km of altitude, (a) and (c), respectively. Time evolution of the sprite signature (i.e., sprite spectra − background spectrum) for an observer located at 40 and 20 km of altitude, (b) and (d), respectively. The absolute sprite spectrum (red curve, graphs a and c) are computed 1 s after the pulse. Thus, it represents the maximum signal.

For the HAPS LOS case (Figures 5c and 5d), the P and R branches of R1 process are still obviously identifiable but the R2 band is split by CO_2 reabsorption between 2,325 and 2,375 cm^{-1}. This is caused by the presence of the highly absorbing lower stratosphere between the observer and the sprite.

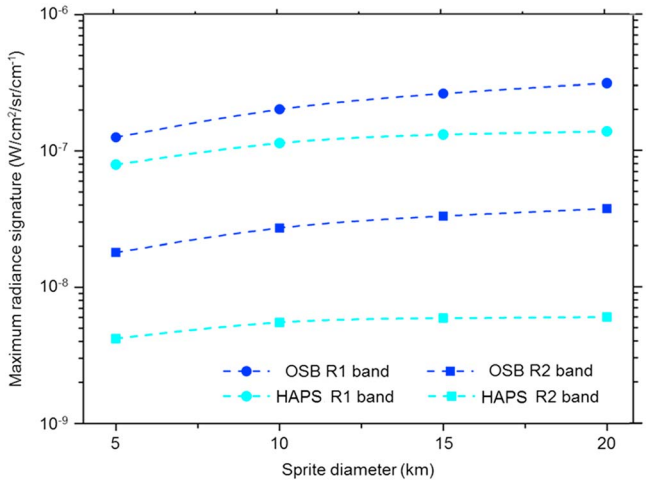

Figure 6. Maximum signature of a sprite as a function of its diameter for observers located in the stratosphere. The OSB and HAPS cases are represented in deep and light blue, respectively. The geometrical setup is the same as previously, likewise the time (1 s after the pulse) and the spectral resolution (1 cm^{-1}). OSA = open stratospheric balloons; HAPS = high-altitude platform system.

The maximum signatures, at 1 s, are about 1.1×10^{-7} and 5.5×10^{-9} W/cm^2/sr/cm^{-1}. At 40 s, the signatures are about 2×10^{-10} and 9×10^{-12} W/cm^2/sr/cm^{-1} in R1 and R2 bands, respectively, which means that the signal decrease is still of almost 3 orders of magnitude in 40 s (Figure 5d).

Considering the uncertainties on the volume of atmosphere exposed to the streamers chemistry, the maximum signatures in R1 and R2 bands are plotted in Figure 6 as a function of the sprite diameter. Except this parameter, the geometry is the same as that used for the previous case (Figure 5).

For the OSB case, from 5 to 20 km of sprite diameter, the maximum signature ranges from 1.2×10^{-7} to 3×10^{-7} W/cm^2/sr/cm^{-1} in R1 band, and 2×10^{-8} to 4×10^{-8} W/cm^2/sr/cm^{-1} in R2 band. Then, for the HAPS case, it ranges from 8.5×10^{-8} to 1.3×10^{-7} W/cm^2/sr/cm^{-1} in R1 band and 4×10^{-9} to 6×10^{-9} W/cm^2/sr/cm^{-1} in R2 band. The effect of the sprite dimension is more appreciable for an observer located at higher altitude (OSB). It should be noted that the variation of the signature with the diameter is not linear. This is due to geometry. To define the distance between the observer and the sprite, the near edge of the cylinder is considered. Thus, as the diameter of the sprite increases, the farthest edge of the cylinder becomes even farther. Then, for the same reason, the LOS,

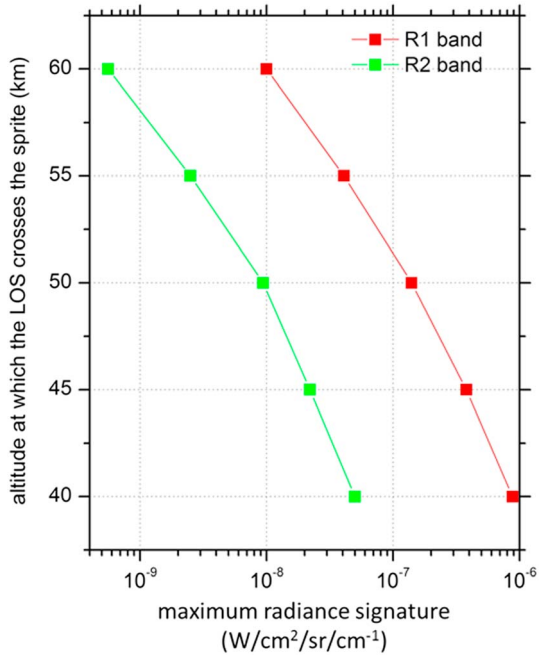

Figure 7. Maximum signature of a sprite as a function of the altitude at which the LOS crosses the sprite-disturbed region. The observer is located at 30 km of altitude, and the zenith angle of the LOS varies so that it crosses the sprite between 40 and 60 km of altitude. The distance is unchanged (d = 50 km), and we kept a sprite diameter of 10 km. LOS = line of sight.

which is oblique, exits the cylinder at a higher altitude. So when the diameter increases, the additional emissions come from a greater distance and higher altitude. They are therefore less intense and more absorbed. Finally, the two spectral ranges do not evolve in the same way because the atmospheric absorption varies with the wavenumber. To summarize, the effect of the sprite diameter on the maximum radiance signature is such that we consider it as a noncritical parameter in the 5- to 20-km range.

The instrument of the HALESIS experiment will be either a multipixel or a spectroimager (Croize et al., 2015). It will be possible to measure the vertical profile of the disturbance and to compare it with background spectra using data from peripheral pixels. Figure 7 shows the vertical profile of the maximum disturbance in the R1 and R2 bands.

The amplitude difference between R1 and R2 bands is always about 1.5 orders of magnitude. Between 40 and 60 km, the signal decrease is as strong as 2 orders of magnitude. The kinetics of vibrational CO_2 involves a different duration of the signature according to the altitude at which the LOS crosses the sprite. At 40 km, where the signature is stronger, its duration will only be about 35 s. This case is given as an illustration, but sprite streamers generally do not develop that low in the stratosphere. At 60 km, the signature could last 80 s due to lower pressure and less efficient quenching (see Figure 4 for CO_2 (001) lifetimes according to the altitude).

According to our model, at 300 km of distance from the sprite, the maximum IR signature could still be about several 1×10^{-8} W/cm^2/sr/cm^{-1} in R1 band and remains 1 order of magnitude lower in the R2 band. Moreover, the embedded instrument will not be optimized to perform such long distance observations which would make it more challenging to set up.

These results legitimate the question of TIR observations from a plane or even from the ground. Figure 8 represents the signatures for observers located at different altitudes: 3 km, which corresponds to several European observatories in the Alps or Pyrenees for example, 5 km (Chilean, Bolivian, and Chinese observatories), and 10 km (plane flight altitude).

The maximum signature in R1 band is of 1.1×10^{-7}, 9.3×10^{-8}, and 7.9×10^{-8} W/cm^2/sr/cm^{-1} for 10, 5, and 3 km of altitude, respectively (Figure 8). This is quite close to OSB and HAPS cases. Even if the absorption is stronger because of the observer altitude, the segment of LOS crossing the sprite is longer due to the narrower zenith angle. Thus, the emission brightness of the source is stronger. Concerning the R2 range, a narrow, quite intense band remains, centered at 2,390 cm^{-1}, and presents a maximum of 3×10^{-9}, 1.3×10^{-9},

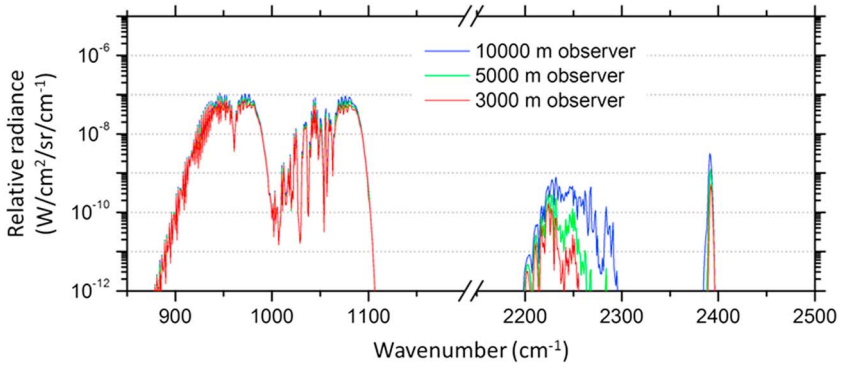

Figure 8. Sprite signatures for observers located in the troposphere. The horizontal distance between observer and sprite is 50 km, and the altitude at which the line of sight crosses the sprite is also 50 km.

and 5×10^{-10} W/cm^2/sr/cm^{-1} (at 10, 5, and 3 km). Between 2,200 and 2,300 cm^{-1}, the effect of atmospheric absorption is clearly visible as the observer is lower and leads to maximum radiances of 8×10^{-10}, 2.9×10^{-10}, and 1.7×10^{-10} W/cm^2/sr/cm^{-1}, respectively.

Increasing the distance of the observer until 300 km (and for h_o = 3 km), the maximum signature in the R1 band regularly decreases to less than 1×10^{-8} W/cm^2/sr/cm^{-1}. In band R2, only two narrow peaks remain: one at 2,220 cm^{-1}, which amplitude is of 1×10^{-11} W/cm^2/sr/cm^{-1}, and the other at 2,390 cm^{-1}, for 2×10^{-11} W/cm^2/sr/cm^{-1}.

4. Conclusions and Perspectives

We highlighted the importance of considering the vibrational kinetics to investigate the IR range. Indeed, the total amount of CO_2 is not affected by a sprite, but the distribution of its vibrational level is, which leads to significant radiative signatures. Then, the principal contributions of this work can be summarized as follows:

- We have confirmed that the IR emissions of sprites come mainly from the strong population of CO_2(001) level.
- There is no significant effect on the production of CO_2 (010, 100) levels.
- According to the altitude at which the LOS crosses the sprite, the signature could persist from 35 s (40 km altitude) to about 100 s (70 km of altitude).
- The LWIR (around 1,000 cm^{-1}) range is the best spectral region to identify the sprite signature since it is highly affected by CO_2(001) emissions and it corresponds to a region where the atmosphere is sufficiently transparent.
- The MWIR (around 2,300 cm^{-1}) range can also be used to identify CO_2(001) emissions but with a signal at least 1 order of magnitude lower than LWIR ones. Indeed, this band is more affected by atmospheric absorption (CO_2 self-trapping and H_2O).
- For an observer located in the troposphere, the LWIR CO_2 emissions should be detectable in standard atmospheric conditions.
- Our computations provide an input to study the detectability of such signatures through different instruments.

The model used here is based on several hypotheses and initial conditions which can affect the output vibrational temperatures of CO_2, and the associated emissions.

- The simulations are done for nighttime (midnight local time) mean summer conditions at 45° of latitude, 0° of longitude.
- The concentrations of excited states are initialized following a Maxwell-Boltzmann distribution (LTE).
- Only first level of each vibrational mode of CO_2 is considered.
- Water vapor chemistry is not included in the kinetics.
- Stationary EEDFs are used to compute electron rate coefficients.
- The concentrations of electrons reached after the passage of a streamer follows the similarity relation in equation (4).
- The reduced electric field during the relaxation is constant and of 30 Td.

Thus, the main perspective of this work is to determine the importance of the different parameters of the model through a sensitivity analysis. This will be presented in an upcoming publication.

Then, the vibrational kinetics will be extended. First, we will evaluate the role of O_2 vibrational levels in the plasma and vibrational kinetics and possible interaction with N_2 and CO_2 vibrational levels. Then, we will investigate the possibility to include NO_x vibrational levels. Indeed, several authors have highlighted the potential production of NO_x caused by sprites (Arnone et al., 2014; Enell et al., 2008; Gordillo-Vázquez, 2008; Hiraki et al., 2008; Nijdam et al., 2010; Peterson et al., 2009; Rodger et al., 2008; Sentman et al., 2008), but, to our knowledge, their vibrational kinetics have never been studied under sprite conditions.

Acknowledgments
The authors wish to acknowledge the French space agency, CNES, the French Aerospace Lab, ONERA, the research and development service of the French army ministry, DGA, that supported this work, and Michael Mills, from the U.S. National Center for Atmospheric Research (NCAR) who provided the WACCM atmospheric composition and temperature profiles used as inputs in this work. The cross-section data for electron collisions used together with the solver BOLSIG+ are from the Itikawa, Morgan (Kinema Research Software), and Phelps databases, www.lxcat.net, retrieved on 5 July 2017.

References

Armstrong, R. A., Shorter, J. A., Taylor, M. J., Suszcynsky, D. M., Lyons, W. A., & Jeong, L. S. (1998). Photometric measurements in the SPRITES'95 &'96 campaigns of nitrogen second positive (399.8 nm) and first negative (427.8 nm) emissions. *Journal of Atmospheric and Solar-Terrestrial Physics*, *60*(7-9), 787–799. https://doi.org/10.1016/S1364-6826(98)00026-1

Arnone, E., Smith, A. K., Enell, C.-F., Kero, A., & Dinelli, B. M. (2014). WACCM climate chemistry sensitivity to sprite perturbations. *Journal of Geophysical Research: Atmospheres*, *119*, 6958–6970. https://doi.org/10.1002/2013JD020825

Baurreau, F., Staraj, R., Ferrero, F., Lizzi, L., Ribero, J. M., & Chessel, J. P. (2015). Stratospheric platform for telecommunication missions. In *2015 IEEE International Symposium on Antennas and Propagation USNC/URSI National Radio Science Meeting* (pp. 914–915). https://doi.org/10.1109/APS.2015.7304844

Bucsela, E., Morrill, J., Heavner, M., Siefring, C., Berg, S., Hampton, D., et al. (2003). $N_2(B^3\Pi_g)$ and $N_2^+(A^2\Pi_u)$ vibrational distributions observed in sprites. *Journal of Atmospheric and Solar-Terrestrial Physics*, *65*(5), 583–590. https://doi.org/10.1016/S1364-6826(02)00316-4

Camy-Peyret, C., Jeseck, P., Hawat, T., Durry, G., Payan, S., Berubé, G., et al. (1995). The LPMA balloon-borne FTIR spectrometer for remote sensing of atmospheric constituents (Vol. 370, p. 323). Presented at the European rocket and balloon programmes and related research. Retrieved from http://adsabs.harvard.edu/abs/1995ESASP.370..323C

Clough, S., Shephard, M., Mlawer, E., Delamere, J., Iacono, M., Cady-Pereira, K., et al. (2005). Atmospheric radiative transfer modeling: A summary of the AER codes. *Journal of Quantitative Spectroscopy and Radiative Transfer*, *91*(2), 233–244. https://doi.org/10.1016/j.jqsrt.2004.05.058

Croize, L., Payan, S., Bureau, J., Duruisseau, F., Thieblemont, R., & Huret, N. (2015). Effect of blue jets on atmospheric composition: Feasibility of measurement from a stratospheric balloon. *IEEE Journal of Selected Topics in Applied Earth Observations and Remote Sensing*, *8*(6), 3183–3192. https://doi.org/10.1109/JSTARS.2014.2381556

d'Oliveira, F. A., de Melo, F. C. L., Devezas, T. C., d'Oliveira, F. A., de Melo, F. C. L., & Devezas, T. C. (2016). High-altitude platforms—Present situation and technology trends. *Journal of Aerospace Technology and Management*, *8*(3), 249–262. https://doi.org/10.5028/jatm.v8i3.699

Enell, C.-F., Arnone, E., Adachi, T., Chanrion, O., Verronen, P. T., Seppälä, A., et al. (2008). Parameterisation of the chemical effect of sprites in the middle atmosphere. *Annales de Geophysique*, *26*(1), 13–27. https://doi.org/10.5194/angeo-26-13-2008

Farges, T., Blanc, E., Hébert, P., Le Mer-Dachard, F., Ravel, K., & Gaillac, S. (2017). MicroCameras and photometers (MCP) on board TARANIS satellite (Vol. 19, p. 6024). Presented at the EGU general assembly conference abstracts. Retrieved from http://adsabs.harvard.edu/abs/2017EGUGA..19.6024F

Franz, R., Nemzek, R., & Winckler, J. (1990). Television image of a large upward electrical discharge above a thunderstorm system. *Science*, *249*(4964), 48–51. https://doi.org/10.1126/science.249.4964.48

Friedl-Vallon, F., Clarmann, T., von Fischer, H., Fritzsche, C., Oelhaf, H., Piesch, C., et al. (1993). Limb emission spectroscopy with the balloon-borne Michelson interferometer for passive atmospheric sounding. In *Optical methods in atmospheric chemistry* (Vol. 1715, pp. 441–451). International Society for Optics and Photonics Environmental Sensing '92, 1992, Berlin, Germany. https://doi.org/10.1117/12.140197

Gordillo-Vázquez, F., Luque, A., & Simek, M. (2012). Near infrared and ultraviolet spectra of TLEs. *Journal of Geophysical Research*, *117*, A05329. https://doi.org/10.1029/2012JA017516

Gordillo-Vázquez, F. J. (2008). Air plasma kinetics under the influence of sprites. *Journal of Physics D: Applied Physics*, *41*(23), 234016. https://doi.org/10.1088/0022-3727/41/23/234016

Hagelaar, G. J. M., & Pitchford, L. C. (2005). Solving the Boltzmann equation to obtain electron transport coefficients and rate coefficients for fluid models. *Plasma Sources Science and Technology*, *14*(4), 722–733. https://doi.org/10.1088/0963-0252/14/4/011

Hampton, D. L., Heavner, M. J., Wescott, E. M., & Sentman, D. D. (1996). Optical spectral characteristics of sprites. *Geophysical Research Letters*, *23*(1), 89–92. https://doi.org/10.1029/95GL03587

Hiraki, Y., Kasai, Y., & Fukunishi, H. (2008). Chemistry of sprite discharges through ion-neutral reactions. *Atmospheric Chemistry and Physics*, *8*(14), 3919–3928. https://doi.org/10.5194/acp-8-3919-2008

Hu, W., Cummer, S. A., & Lyons, W. A. (2007). Testing sprite initiation theory using lightning measurements and modeled electromagnetic fields. *Journal of Geophysical Research*, *112*, D13115. https://doi.org/10.1029/2006JD007939

Lefeuvre, F., Blanc, E., Pinçon, J.-L., Roussel-Dupré, R., Lawrence, D., Sauvaud, J.-A., et al. (2008). TARANIS—A satellite project dedicated to the physics of TLEs and TGFs. *Space Science Reviews*, *137*(1-4), 301–315. https://doi.org/10.1007/s11214-008-9414-4

Marsh, D. R., Mills, M. J., Kinnison, D. E., Lamarque, J.-F., Calvo, N., & Polvani, L. M. (2013). Climate change from 1850 to 2005 simulated in CESM1(WACCM). *Journal of Climate*, *26*(19), 7372–7391. https://doi.org/10.1175/JCLI-D-12-00558.1

Mende, S. B., Rairden, R. L., Swenson, G. R., & Lyons, W. A. (1995). Sprite spectra; N_2 1 PG band identification. *Geophysical Research Letters*, *22*(19), 2633–2636. https://doi.org/10.1029/95GL02827

Milikh, G. M., Usikov, D. A., & Valdivia, J. A. (1998). Model of infrared emission from sprites. *Journal of Atmospheric and Solar-Terrestrial Physics*, *60*(7–9), 895–905. https://doi.org/10.1016/S1364-6826(98)80009-6

Morrill, J. S., Bucsela, E. J., Pasko, V. P., Berg, S. L., Heavner, M. J., Moudry, D. R., et al. (1998). Time resolved N_2 triplet state vibrational populations and emissions associated with red sprites. *Journal of Atmospheric and Solar-Terrestrial Physics*, *60*(7-9), 811–829. https://doi.org/10.1016/S1364-6826(98)00031-5

Nijdam, S., van Veldhuizen, E. M., & Ebert, U. (2010). Comment on "NO_x production in laboratory discharges simulating blue jets and red sprites" by H. Peterson et al. *Journal of Geophysical Research*, *115*, A12305. https://doi.org/10.1029/2010JA015861

Pancheshnyi, S., Eismann, B., Hagelaar, G. J. M., & Pitchford, L. C. (2008). ZDPlasKin|Zero-dimensional plasma kinetics solver. Retrieved November 29, 2016, from http://www.zdplaskin.laplace.univ-tlse.fr/

Parra-Rojas, F. C., Luque, A., & Gordillo-Vázquez, F. J. (2015). Chemical and thermal impacts of sprite streamers in the Earth's mesosphere. *Journal of Geophysical Research: Space Physics*, *120*, 8899–8933. https://doi.org/10.1002/2014JA020933

Pasko, V. P. (2010). Recent advances in theory of transient luminous events. *Journal of Geophysical Research*, *115*, A00E35. https://doi.org/10.1029/2009JA014860

Pasko, V. P., Stanley, M. A., Mathews, J. D., Inan, U. S., & Wood, T. G. (2002). Electrical discharge from a thundercloud top to the lower ionosphere. *Nature*, *416*(6877), 152–154. https://doi.org/10.1038/416152a

Pasko, V. P., & Stenbaek-Nielsen, H. C. (2002). Diffuse and streamer regions of sprites. *Geophysical Research Letters*, *29*(10), 1440. https://doi.org/10.1029/2001GL014241

Pasko, V. P., Yair, Y., & Kuo, C.-L. (2012). Lightning related transient luminous events at high altitude in the Earth's atmosphere: Phenomenology, mechanisms and effects. *Space Science Reviews*, *168*(1–4), 475–516. https://doi.org/10.1007/s11214-011-9813-9

Peterson, H., Bailey, M., Hallett, J., & Beasley, W. (2009). NO_x production in laboratory discharges simulating blue jets and red sprites. *Journal of Geophysical Research*, *114*, A00E07. https://doi.org/10.1029/2009JA014489

Picard, R., Inan, U., Pasko, V., Winick, J., & Wintersteiner, P. (1997). Infrared glow above thunderstorms? *Geophysical Research Letters*, *24*(21), 2635–2638. https://doi.org/10.1029/97GL02753

Qin, J., & Pasko, V. P. (2015). Dynamics of sprite streamers in varying air density. *Geophysical Research Letters*, *42*, 2031–2036. https://doi.org/10.1002/2015GL063269

Rodger, C. J., Seppälä, A., & Clilverd, M. A. (2008). Significance of transient luminous events to neutral chemistry: Experimental measurements. *Geophysical Research Letters*, *35*, L07803. https://doi.org/10.1029/2008GL033221

Sentman, D., Stenbaek-Nielsen, H., McHarg, M., & Morrill, J. (2008). Plasma chemistry of sprite streamers. *Journal of Geophysical Research*, *113*, D11112. https://doi.org/10.1029/2007JD008941

Sentman, D. D., Wescott, E. M., Osborne, D., Hampton, D., & Heavner, M. (1995). Preliminary results from the Sprites94 aircraft campaign: 1. Red sprites. *Geophysical Research Letters*, *22*(10), 1205–1208. https://doi.org/10.1029/95GL00583

Siefring, C. L., Morrill, J. S., Sentman, D. D., & Heavner, M. J. (2010). Simultaneous near-infrared and visible observations of sprites and acoustic-gravity waves during the EXL98 campaign. *Journal of Geophysical Research*, *115*, A00E57. https://doi.org/10.1029/2009JA014862

Wilson, C. T. R. (1924). The electric field of a thundercloud and some of its effects. *Proceedings of the Physical Society of London*, *37*(1), 32D–37D. https://doi.org/10.1088/1478-7814/37/1/314